STRUCTURAL BIOLOGY COMMUNICATIONS

ISSN 2053-230X

A sucrose-binding site provides a lead towards an isoform-specific inhibitor of the cancer-associated enzyme carbonic anhydrase IX

Melissa A. Pinard,[a] Mayank Aggarwal,[b] Brian P. Mahon,[a] Chingkuang Tu[c] and Robert McKenna[d]*

[a]Department of Biochemistry and Molecular Biology, College of Medicine, University of Florida, Gainesville, FL 32610, USA, [b]Division of Biology and Soft Matter, Oak Ridge National Laboratory, Oak Ridge, TN 37831, USA, [c]Department of Pharmacology, College of Medicine, University of Florida, Gainesville, FL 32610, USA, and [d]Department of Biochemistry and Molecular Biology, College of Medicine, University of Florida, Gainesville, FL 32610, USA. *Correspondence e-mail: rmckenna@ufl.edu

Received 17 April 2015
Accepted 27 June 2015

Edited by N. Sträter, University of Leipzig, Germany

Keywords: α-carbonic anhydrase; CA IX mimic; isoform-specific drug design; sugar approach; carbonic anhydrase IX; sucrose.

PDB reference: complex with sucrose, 4ywp

Supporting information: this article has supporting information at journals.iucr.org/f

Human carbonic anhydrase (CA; EC 4.2.1.1) isoform IX (CA IX) is an extracellular zinc metalloenzyme that catalyzes the reversible hydration of CO_2 to HCO_3^-, thereby playing a role in pH regulation. The majority of normal functioning cells exhibit low-level expression of CA IX. However, in cancer cells CA IX is upregulated as a consequence of a metabolic transition known as the Warburg effect. The upregulation of CA IX for cancer progression has drawn interest in it being a potential therapeutic target. CA IX is a transmembrane protein, and its purification, yield and crystallization have proven challenging to structure-based drug design, whereas the closely related cytosolic soluble isoform CA II can be expressed and crystallized with ease. Therefore, we have utilized structural alignments and site-directed mutagenesis to engineer a CA II that mimics the active site of CA IX. In this paper, the X-ray crystal structure of this CA IX mimic in complex with sucrose is presented and has been refined to a resolution of 1.5 Å, an R_{cryst} of 18.0% and an R_{free} of 21.2%. The binding of sucrose at the entrance to the active site of the CA IX mimic, and not CA II, in a non-inhibitory mechanism provides a novel carbohydrate moiety binding site that could be further exploited to design isoform-specific inhibitors of CA IX.

1. Introduction

In many metastatic tumors, the rapidly proliferating cancer cells create an extracellular milieu that is characterized by a reduction in overall oxygen content (≤1.0%) and the acidification of the extracellular environment (Moulder & Rockwell, 1987; Peskin & Carter, 2008). This condition is termed tumor hypoxia and is owing to an imbalance between the demand of the proliferating cancer cells for oxygen and the capabilities of the vascular system surrounding them to supply it (Mahon & McKenna, 2013). As a result of hypoxic stress, tumor cells shift their energetic metabolism from mitochondrial oxidative phosphorylation to anaerobic glycolysis in the cytosol, a phenomenon known as the Warburg effect (Vander Heiden *et al.*, 2009). This results in an increased amount of lactic acid being exported from the cells, leading to a decrease in the extracellular pH (pHe ∼6.5) and the upregulation of pH homeostasis factors that control the extracellular/intracellular pH (pHe/pHi) gradient (Racker, 1981).

Humans express 15 α-class carbonic anhydrase (CA) isoforms, each with numerous physiological roles and variable expression patterns, of which 12 are catalytically active and

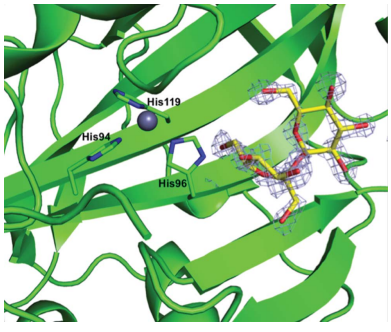

catalyze the reversible hydration of CO_2 to HCO_3^- (Frost, 2014). Two of these CAs (CA IX and XII), which are both extracellular, have been identified as being tumor-associated and play a role in the pH homeostasis of cancer cells (Liao *et al.*, 2009; Benej *et al.*, 2014). However, CA IX has been shown to be more prevalent in solid tumors compared with CA XII (Benej *et al.*, 2014). In a non-disease state CA IX is almost exclusively expressed in the gut epithelium (Pastoreková *et al.*, 1997; Liao *et al.*, 2009; McDonald *et al.*, 2012), but it is ectopically expressed in several tumors (including breast, liver, lung, colon/rectum and head/neck) in response to hypoxia (Wykoff *et al.*, 2000; Mahon & McKenna, 2013). The major regulator of CA IX expression is hypoxia-induced factor 1, the upregulation of which is associated with hypoxia-responsive elements and the overall progression of cancer (Luo *et al.*, 2014). As such, CA IX activity has been shown to be an important regulatory factor for tumor cells to maintain an acidic pHe yet to have a near-physiological pHi (Mahon *et al.*, 2015). The limited expression of CA IX in healthy cells and its aberrant expression in numerous tumor types has led to its establishment as a general marker of tumor hypoxia as well as a potential drug-therapy target (Mahon & McKenna, 2013).

The inhibition mechanism of CA inhibitors (CAIs) is well established and sulfonamides are regarded as the most potent class of inhibitors. However, current CAIs are not specific owing to structural homology and high amino-acid conservation among CA isoforms (Aggarwal, Kondeti *et al.*, 2013). Thus, they bind indiscriminately to CAs that are more abundant in the cytosol, such as CAs I, II and III (Tafreshi *et al.*, 2012). In contrast, the catalytic domain of CA IX faces the extracellular milieu and presents an alternative method of targeting the enzyme in tumor cells (Barathova *et al.*, 2008; Hilvo *et al.*, 2008; Pinard *et al.*, 2015). The incorporation of bulky membrane-impermeable chemical moieties appended to classic CAIs such as acetazolamide (AZM) or cationic sulfonamide derivatives is one such strategy (Mahon & McKenna, 2013).

A more recent class of CAIs, glycoconjugated sulfonamides, utilizes derivatives of the sulfonamide zinc-binding group (ZBG), for example secondary cyclic sulfonamides or benzene sulfonamides appended to a monosaccharide or disaccharide tail. The ZBG allows the CAI to bind directly to the zinc ion as seen in classical CAIs, while the bulky sugar moiety allows the CAI to maintain water solubility and maintain bioavailability (Meyer *et al.*, 2011; Carroux *et al.*, 2013). However, unlike previous designed bulky sulfonamide compounds, the high molecular weight of the glycoconjugated sulfonamides confers membrane impermeability onto the CAI. Moreover, studies have already shown that these CAIs show a >1000-fold selectivity for CA IX over CA II (Siebels *et al.*, 2011; Moeker *et al.*, 2014; Mahon *et al.*, 2015).

At present, only one crystal structure of the catalytic domain of CA IX exists, with AZM. Despite the exploitation of structure-based drug design for other protein systems, difficulties in the expression and crystallization of CA IX have hindered the study of CA IX–inhibitor complexes. To overcome this, our group has engineered a CA IX mimic by mutating seven positionally equivalent amino acids in the active site (A65S, N67Q, E69T, I91L, F131V, K170E and L204A) using the cDNA of the much more easily crystallizable CA II as a structural template.

During efforts to study the structures of the CA IX mimic in complex with inhibitors using sucrose as a cryoprotectant, sucrose was serendipitously found to bind near the entrance to the active site of the CA IX mimic but not of CA II. The rationale for not using the more conventional glycerol as a cryoprotectant was its observed binding in the active site of CA II and therefore its possible effect on inhibitor binding (Aggarwal, Kondeti *et al.*, 2013). Following this observation of a well ordered sucrose in the X-ray crystal structure of the CA IX mimic, binding studies using differential scanning fluorimetry (DSF) of sucrose in complex with CA II, the CA IX mimic and wild-type CA IX were performed. DSF studies of glucose and fructose, the monosaccharides constituting sucrose, in complex with CA II, the CA IX mimic and wild-type CA IX were also carried out for comparison.

Taken together, these data provide a detailed understanding of CA isoform-selective binding of sucrose near the active-site mouth and provide insight into the development of CAIs that incorporate a soluble sucrose moiety. Furthermore, the use of sucrose-based glycoconjugates over monosaccharides such as glucose or fructose would circumvent the issue of interactions with specific transporters since humans lack sucrose transporters.

2. Materials and methods

2.1. Expression and purification of the CA IX mimic and CA II

The CA IX mimic was prepared by site-directed mutagenesis of seven residues, A65S, N67Q, E69T, I91L, F131V, K170E and L204A, with the QuikChange mutagenesis kit from Stratagene using a CA II cDNA template. The DNA sequence was then confirmed for the entire coding region for the CA in the expression vector (Genis *et al.*, 2009). The expression and purification of the CA IX mimic and CA II were performed as described previously (Pinard *et al.*, 2013). A final protein concentration of $\sim$10 mg ml^{-1} was calculated for each protein by measuring the optical density at 280 nm and using a molar absorptivity of $5.4 \times 10^4\ M^{-1}\ cm^{-1}$.

2.2. Expression and purification of CA IX

A bacmid containing CA IX was graciously provided by our collaborators, Claudiu T. Supuran (University of Florence, Italy) and Seppo Parkkila (University of Tampere, Finland), and was optimized for *Spodoptera frugiperda* (Sf9) cells. The CA IX construct contained amino acids 1–377, which make up the catalytic domain (CA), the proteoglycan domain (PG) and a signal peptide linked to a poly-(8×)-histidine tag, similar to as described in Hilvo *et al.* (2008) and Alterio *et al.* (2009). CA IX was expressed using a baculovirus expression system (Invitrogen; Patterson *et al.*, 1995). 1 l of Sf9 cells were grown in Sf-900 II SFM medium (Life Technologies, New York, USA) to a density of 2.0×10^6 cells ml^{-1} and were infected

Table 1
X-ray crystallographic data-collection and refinement statistics.

Values in parentheses are for the highest resolution bin.

	CA IX mimic–sucrose	CA IX mimic
PDB code	4ywp	4zao
Data-collection statistics		
Temperature (K)	100	100
Wavelength (Å)	0.918	1.54
Space group	$P2_1$	$P2_1$
Unit-cell parameters		
a (Å)	41.8	41.8
b (Å)	41.2	41.2
c (Å)	72.3	72.0
β (°)	103.8	103.8
Reflections		
Theoretical	42836	22290
Unique	42193	21707
Resolution (Å)	20.0–1.50 (1.50–1.45)	20.0–1.80 (1.86–1.80)
R_{merge}† (%)	5.1 (10.3)	4.5 (6.3)
$\langle I/\sigma(I)\rangle$	16.3 (11.7)	17.3 (12.8)
Completeness (%)	98.5 (99.7)	97.5 (97.1)
Multiplicity	3.7 (3.5)	2.7 (2.7)
Model statistics		
R_{cryst}‡ (%)	18.0	17.5
R_{free}§ (%)	21.2	20.5
Residue Nos.	4–261	4–261
No. of atoms¶		
Protein	2132	2132
Ligand	27	0
Water	290	169
R.m.s.d.		
Bond lengths (Å)	0.009	0.006
Bond angles (°)	1.32	1.044
Ramachandran statistics (%)		
Favored	89.0	94.8
Allowed	11.0	5.2
Average B factors (Å^2)		
Main chain	9.5	13.9
Side chain	13.4	18.6
Ligand	7.8	—
Solvent	19.9	23.8

† $R_{merge} = \sum_{hkl}\sum_i |I_i(hkl) - \langle I(hkl)\rangle| / \sum_{hkl}\sum_i I_i(hkl) \times 100$. ‡ $R_{cryst} = \sum_{hkl} ||F_{obs}| - |F_{calc}|| / \sum_{hkl} |F_{obs}| \times 100$. § R_{free} is calculated in the same manner as R_{cryst} except that it uses 5% of the reflection data omitted from refinement. ¶ Includes alternate conformations.

with baculovirus containing CA IX bacmid using a multiplicity of infection (MOI) of 5. The cells were then harvested by centrifugation after 72 h. Supernatant containing CA IX was diluted twofold in 20 m*M* sodium phosphate, 500 m*M* NaCl, 15 m*M* imidazole pH 7.8 and was purified by nickel column chromatography in a gravity column containing 15 ml Ni–NTA agarose (Life Technologies; Hilvo *et al.*, 2008). Eluent containing CA IX was then concentrated by centrifugation to a total volume of 500 µl. The poly-(8×)-histidine tag was removed from the concentrated CA IX sample using a Thrombin CleanCleave Kit based on the manufacturer's guidelines (Life Technologies). After removal of the poly-(8×)-histidine tag, the sample of CA IX was further purified and buffer-exchanged (50 m*M* Tris, 150 m*M* NaCl pH 7.4) by size exclusion using an ÄKTA pure protein-purification system (GE Healthcare) equipped with a Superdex 200 10/300 GL gel-filtration column (GE Healthcare). The eluted sample was collected in 1 ml fractions. The chromatogram (absorbance at 280 nm) of eluted CA IX revealed two individual peaks indicative of populations of monomeric and dimeric units (not shown). Peak fractions from both monomers and dimers of CA IX were pooled and concentrated by centrifugation. The final concentration of purified CA IX was estimated to be 3 mg ml^{-1} by UV–Vis spectroscopy (Gill & von Hippel, 1989) using an extinction coefficient of 5.2 × 10^4 M^{-1} cm^{-1}.

2.3. Crystallization

Crystals of CA II and the CA IX mimic were grown at room temperature using the sitting-drop vapor-diffusion method. A crystallization screen was made using the Crystal Gryphon automated system (Art Robbins) with conditions ranging from 1.1 to 1.7 *M* sodium citrate and 50 m*M* Tris–HCl pH 7.0–9.0 as the precipitant solution. Crystals were obtained by mixing 0.3 µl protein solution (∼10 mg ml^{-1} in 50 m*M* Tris–HCl pH 7.8) with 0.3 µl precipitant solution. The drops were equilibrated against 60 µl precipitant solution. Crystals appeared within 7 d. Crystals formed using 1.6 *M* sodium citrate, 50 m*M* Tris–HCl pH 7.5 were used for data collection.

2.4. Diffraction data collection

X-ray diffraction data were collected on Cornell High Energy Synchrotron Source (CHESS) beamline F1 using an ADSC Quantum 210 detector at a wavelength of 0.918 Å. Crystals of CA II and the CA IX mimic were immersed in 20%(*w*/*v*) sucrose (∼0.6 *M*) cryoprotectant for approximately 5 s and immediately flash-cooled at 100 K for data collection. A total of 360 frames with an oscillation range of 0.5° each were collected with an exposure of 5 s. The data were indexed, integrated and scaled using *HKL*-2000 (Otwinowski & Minor, 1997). Diffraction data statistics for the CA IX mimic in complex with sucrose are highlighted in Table 1. In an attempt to complex sucrose to CA II, these soaks were repeated three more times, but this proved futile despite increasing the concentration of sucrose to 1.0 *M*.

2.5. Model refinement

The initial phases were calculated using PDB entry 3ks3 (Avvaru *et al.*, 2010) with waters removed and the residues unique to the CA IX active site (Ser65, Gln67, Thr69, Leu91, Val131, Leu135 and Glu170) mutated to alanines. The auto molecular-replacement (*AutoMR*) procedure in the *PHENIX* suite of programs (Adams *et al.*, 2010) was used to carry out molecular replacement. The structure was refined using the *PHENIX* software suite (Adams *et al.*, 2010) and manual refitting of the model based on the electron-density map was performed in the graphics program *Coot* (Emsley & Cowtan, 2004). A topology file for sucrose was generated using the *PRODRG* server (Schüttelkopf & van Aalten, 2004) and this file was used to model the sugar into the difference electron-density map ($F_{obs} - F_{calc}$). Iterative refinement of the structure was performed until the R_{work} and R_{free} were minimized and were within 5% of each other. *PROCHECK* (Laskowski *et al.*, 1993) was then used to analyze the geometric restraints of the final model; the final model refinements are summarized in Table 1.

2.6. Enzyme kinetics

^{18}O-Exchange mass spectrometry was used to measure the catalytic rate of the dehydration of HCO_3^- to CO_2 by the CA IX mimic in the presence of 2 *M* sucrose at 283 K using ^{18}O-labeled HCO_3^- as described previously (Silverman *et al.*, 1980). In the first step of catalysis there is a random probability of labeling the active site of the enzyme with ^{18}O (1). In the second step the protonation of the zinc-bound $^{18}OH^-$ *via* His64 results in the release of $H_2^{18}O$ into the bulk solvent. This method is dependent on the depletion of ^{18}O from CO_2 in solution. As the CO_2 enters the semi-permeable membrane of an Extrel EXM-200 mass spectrometer, its ^{18}O-labeled isotopic content is measured.

$$\begin{aligned} HCOO^{18}O^- + EZn_2O &\rightarrow EZnHCOO^{18}O \\ &\rightarrow CO_2 + EZn^{18}OH^-, \end{aligned} \quad (1)$$

$$\begin{aligned} H^+His64\text{-}EZn^{18}OH^- &\rightleftharpoons His64\text{-}EZnH_2^{18}O^- \\ &\rightarrow His64\text{-}EZnH_2O + H_2^{18}O. \end{aligned} \quad (2)$$

2.7. Differential scanning fluorimetry stability assay

Samples of CA II, the CA IX mimic and CA IX (at 0.25 mg ml^{-1}) were incubated with varying sucrose concentrations from 0.1 to 1.0 *M* for 1 h in a 1:1(*v*:*v*) ratio. 2.5 µl of 1% SYPRO Orange dye (catalog No. S6651; Invitrogen Inc.) was added to each protein–ligand sample to bring the final volume of each reaction to 25 µl. The assays were conducted in a quantitative PCR (qPCR) instrument (RG-3000; Corbett Research) with temperature ramping from 30 to 99°C, increasing at the rate of 0.1°C every 6 s. Control samples of protein only at a concentration of 0.25 mg ml^{-1} were included in each run as a positive control. The melting temperature (T_m) was defined as the maximum value of the first derivative (dF/dT; change in fluorescence/change in temperature) of the signal.

3. Results and discussion

3.1. Crystallographic studies

The CA IX mimic–sucrose complex crystal diffracted to 1.5 Å resolution and belonged to space group $P2_1$, with unit-cell parameters a = 41.8, b = 41.2, c = 72.1 Å, β = 103.8°. The structure was refined to an R_{cryst} and R_{free} of 18.0 and 21.2%, respectively. Other structural details are summarized in Table 1. An initial $F_o - F_c$ map clearly showed a sucrose molecule bound near the entrance to the CA IX mimic active site (Fig. 1). The sucrose molecule interacts mostly with the residues forming the hydrophilic cleft, Asn62, His64, Gln67 and Gln92, and when superimposed onto an unbound CA IX mimic structure (PDB entry 4zao) showed that no ordered water molecules are displaced upon sucrose binding (Fig. 2). The sucrose makes significant hydrogen bonds to numerous

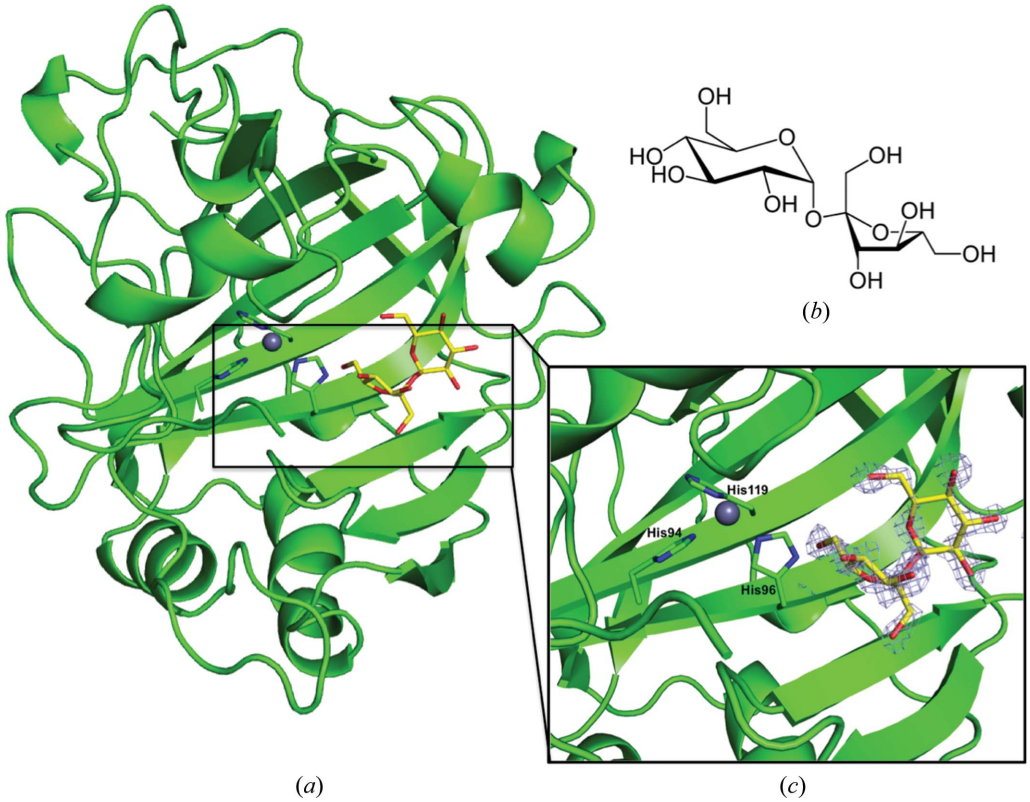

Figure 1
(*a*) Cartoon representation of the CA IX mimic in complex with sucrose. The gray sphere coordinated by three histidine residues represents the zinc ion. The electron density (grey mesh; $2F_o - F_c$ Fourier map) is contoured at 1.3σ. (*b*) Structure of sucrose. (*c*) Enlarged view of the CA IX mimic–sucrose complex.

solvent molecules within the active site, including those making up the conserved ordered water network observed in the unbound active site, further stabilizing the molecule in the active site (Mikulski *et al.*, 2013). Weak van der Waals interactions were also seen between the sucrose and the side chains of Leu91 and Val131 from the hydrophobic cleft. Both of these residues are present in CA IX but not in CA II (Fig. 2).

Sucrose could also serve as a potential ligand for CA II, but multiple attempts to crystallize CA II in the presence of sucrose proved futile, making sucrose an even more attractive isoform-specific ligand for CA IX since it appears to have low affinity for the off-target CA II.

3.2. Kinetics and differential scanning fluorimetry (DSF)

An inhibition constant for sucrose could not be measured since sucrose does not inhibit the enzymes. The ligand binds at the entrance to the active site, away from the substrate-binding site (PDB entry 3d92; Domsic *et al.*, 2008), and does not disrupt the ordered water network (Mikulski *et al.*, 2013).

Thermal stability assays were carried out using DSF for CA II, the CA IX mimic and CA IX in complex with sucrose, glucose and fructose. CA II exhibited the smallest change in T_m among the three proteins, exhibiting a ΔT_m of 3°C (Fig. 3*a*). Similarly, a ΔT_m of 3.5°C was observed for the CA IX mimic (Fig. 3*b*), while CA IX showed the largest ΔT_m of 5°C (Fig. 3*c*). The T_m values for each protein at the different sucrose concentrations given in Supplementary Table S1 indicate that increasing concentrations of sucrose stabilize each of these proteins. A set of distinct peaks were observed in the thermogram for CA IX (Fig. 3*c*); unlike CA II and the CA IX mimic, CA IX is a dimer and consists of two domains. The two peaks indicate two different T_m values owing to the unfolding of its different domains independently of each other. As mentioned previously, the catalytic domain of CA IX displays structural homology to those of the other α-CAs. Hence, at each sucrose concentration the initial (lower) T_m is owing to the unfolding of the catalytic domain (similar in sequence to CA II), while the second (higher) T_m is most likely owing to the unfolding of the proteoglycan domain of the enzyme. An alternative explanation is that these distinct peaks could be owing to the exposure of the hydrophobic dimer interface as the dimer separates and the enzyme is denatured.

To estimate the dissociation constant (K_d) of each sugar for either CA II, the CA IX mimic or CA IX, a simple saturation model was used. For some enzyme–ligand complexes saturation was not achieved and so an exact K_d could not be determined. A K_d of 0.08 ± 0.04 *M* was observed for CA IX in

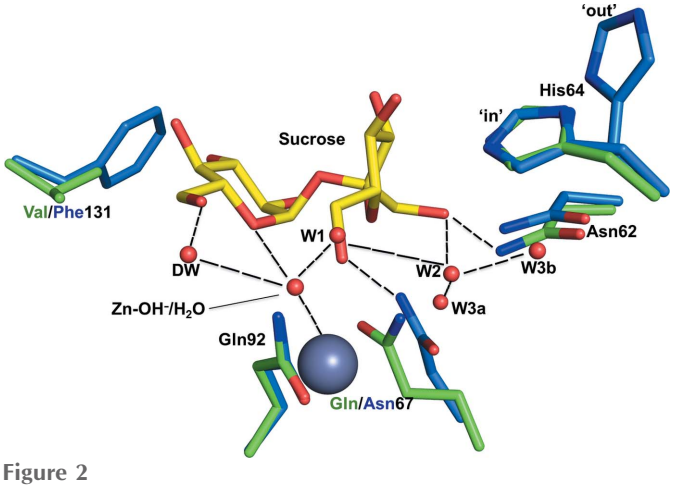

Figure 2
Overlay of interfacing residues in the CA IX mimic–sucrose crystal structure (green) and CA II (blue), showing conservation of the ordered water network in the CA IX mimic.

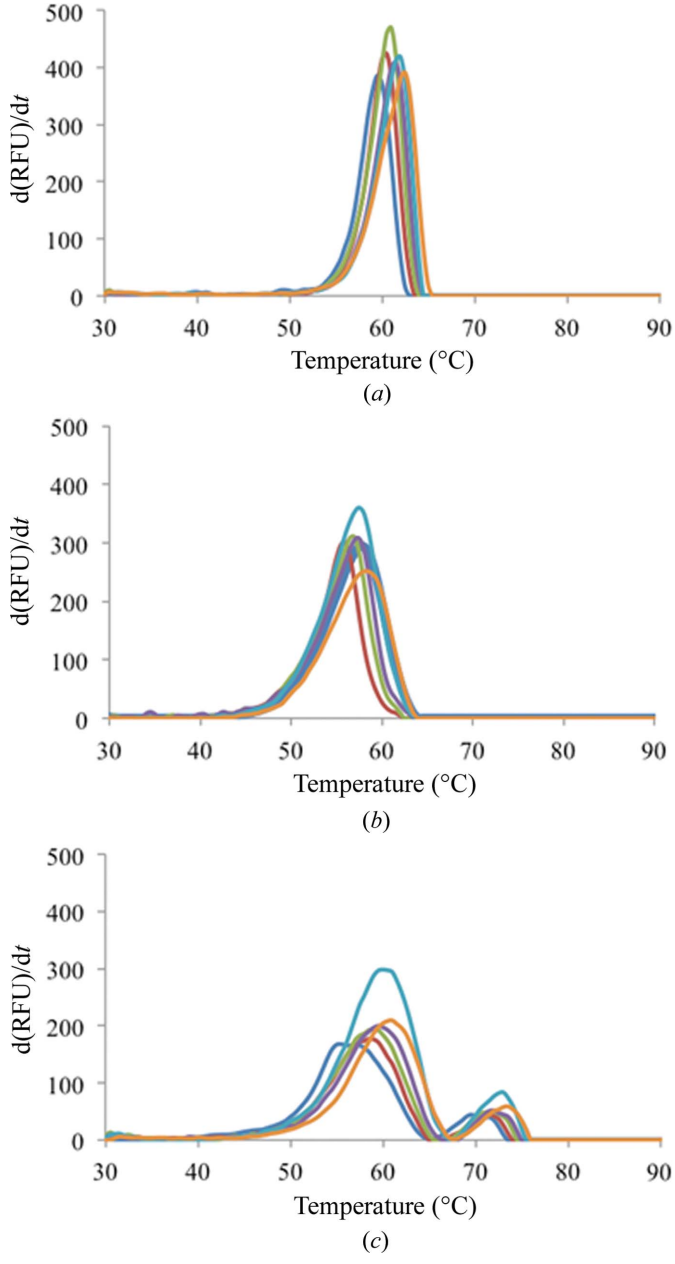

Figure 3
DSF measurements of fluorescence intensity during heating of (*a*) CA II, (*b*) the CA IX mimic and (*c*) CA IX in the presence of varying concentrations of sucrose. For each isoform, the data are normalized averages from three temperature-scan experiments. Each color represents a scan carried out at a different sucrose concentration (blue, 0.0 *M*; red, 0.2 *M*; green, 0.4 *M*, purple, 0.6 *M*; cyan, 0.8 *M*; orange, 1.0 *M*).

complex with sucrose as well as in complex with fructose. CA IX appears to have less affinity for glucose; the enzyme never fully saturated. For the CA IX mimic in complex with sucrose a K_d of 1.2 ± 0.8 *M* was calculated.

One possible explanation for the similarity in the K_d values for sucrose and fructose for both CA IX and the CA IX mimic could be inferred from the crystal structure of the CA IX mimic in complex with sucrose. When sucrose binds at the mouth of the active site, its fructose component binds closest to the active-site zinc (∼5 Å) and the fructose moiety makes the majority of its interactions with water molecules and amino acids in the active site (Fig. 2). On the other hand, the sucrose moiety extends out of the active site and interacts with a few sparse water molecules and makes weak interactions with Val131 and Leu91.

In the case of the CA II complexes, all of the sugars exhibited very little affinity for the enzyme. The enzyme was never saturated and no K_d was calculated for CA II in complex with sucrose. Superimpositions of CA II onto the CA IX mimic–sucrose complex (r.m.s.d. of 0.4 Å) shows that the bulky side chain of Phe131 (compared with Val131 in the CA IX mimic) would interfere with sucrose binding, creating steric hindrance. This could be a possible explanation why sucrose is not able to bind in CA II. Another interesting interaction that sucrose makes is that with Gln67 in the CA IX mimic compared with Asn67 in CA II (Fig. 2). Glutamic acid contains an extra $-CH_2$, which allows it to make two hydrogen bonds compared with the shorter Asn67 in CA II, which would probably only make one bond. This could be yet another reason for preferential binding.

4. Conclusion

The sugar approach to CA inhibition has become more popular with the search for more selective CA isoform inhibitors. The classical low-molecular-weight CAIs bind deep into the CA active-site cavity and make limited interactions with the amino acids that differ between isoforms in the hydrophilic and hydrophobic cleft surrounding the active site of the enzyme. These CAIs are mostly sulfonamides and, although potent inhibitors, they exhibit indiscriminatory inhibition profiles among the different isoforms. One way to overcome this difficulty and create isoform-selective CAIs is to elongate these inhibitors by using the 'tail approach' to append tails that will make extensive interactions with the surrounding amino acids to the ZBG moieties (Supuran, 2012). Additionally, linking a sugar moiety to a sulfonamide scaffold would alter the properties of this drug, making it more soluble yet impermeable to the cell membrane, thus eliminating any off-target effects.

The glycoconjugate class of inhibitors utilizes this approach, and in these compounds either a sulfonamide or sulfamate group is bound to the anomeric C atom of a carbohydrate. This class of inhibitors has been used primarily against the tumor-associated CA IX and XII. Initial studies carried out by the Poulsen group by screening anomeric sulfonamides using the CO_2 hydration assay against the cytosolic CAs I and II, and the tumor-associated CAs IX and XII, showed that these inhibitors show no isoform selectivity (Lopez *et al.*, 2009; Métayer *et al.*, 2013). However, these studies did not include the use of sucrose as a carbohydrate. The anomeric sulfamides were shown to be much better CA IX inhibitors, with inhibition constants below 8 n*M* and with selectivity over CA I (480-fold to 1800-fold) and CA II (∼17-fold) (Winum *et al.*, 2013). A third class of sugar inhibitors, the 6-sulfamoyl carbohydrates, are synthesized from monosaccharides or disaccharides through the selective sulfamoylation of the C6 hydroxyl group (Lopez *et al.*, 2011). Studies by the Poulsen group have also shown that glucose derivatives were more selective inhibitors (in the nanomolar range) of CA IX (eightfold to 14-fold) compared with CA II (Lopez *et al.*, 2011). A potential inhibitor could incorporate sucrose by sulfamoylation of its C6 hydroxyl group. Therefore, the addition of a ZBG derivative to the sucrose moiety could prove to be a formidable anticancer drug, and the use of structure-based drug design in an attempt to exploit the subtle differences between active sites of CAs would be critical in this effort.

The bound sucrose molecule (Fig. 2) gives insights into possible drug-design strategies using the 'sugar approach', which entails attaching a molecule moiety (acting as a 'tail') to a known high-affinity zinc-binding motif. The DSF data suggest that the fructose component is what confers specificity and so the addition of a short linker between the fructose component and a potential ZBG would be one option. In addition, the crystal structure shows that the fructose component points towards the active site, while the glucose moiety extends out of the active site. The development of a drug that can selectively inhibit CA IX over off-target cytosolic CAs could be critical in slowing down tumor cell survival in the microenvironment created under hypoxic conditions. The potency and success of such a drug will be dependent on the interaction of its tail moiety with the residues near the active site. The mouth of a CA active site is the most variable region among the different isoforms and studies have shown that these 'tails' bind in these regions and could potentially lead to the development of isoform-selective CAIs (Aggarwal, Boone *et al.*, 2013; Aggarwal, Kondeti *et al.*, 2013).

Currently, the disaccharides being used in the synthesis of glycoconjugates utilize a galactose moiety and show stronger inhibition for CA II compared with CA IX. Although these compounds do not cross the membrane, they appear to be weak CA IX binders and so may not be valid drug candidates. Furthermore, although glycoconjugates constituting glucose moieties show stronger inhibition of CA IX *versus* CA II and present a lot of promise, these CAIs may unintentionally interact with glucose transporters in the body. Therefore, utilization of the disaccharide sucrose may prove to be a better option since humans lack a sucrose transporter, and our preliminary data already indicate that sucrose shows a preference for CA IX over CA II.

Acknowledgements

This work was supported by a grant from the NIH (GM25154). RM would like to thank the Center of Structural Biology for

support of the X-ray facility at UF. We would also like to thank the MacCHESS staff for their help during X-ray diffraction data collection at the Cornell High Energy Synchrotron (CHESS) Facility, Ithaca. MA is funded by the Department of Energy and Shull Fellowship at Oak Ridge National Laboratory.

References

Adams, P. D. *et al.* (2010). *Acta Cryst.* D**66**, 213–221.

Aggarwal, M., Boone, C. D., Kondeti, B. & McKenna, R. (2013). *J. Enzyme Inhib. Med. Chem.* **28**, 267–277.

Aggarwal, M., Kondeti, B. & McKenna, R. (2013). *Bioorg. Med. Chem.* **21**, 1526–1533.

Alterio, V., Hilvo, M., Di Fiore, A., Supuran, C. T., Pan, P., Parkkila, S., Scaloni, A., Pastorek, J., Pastorekova, S., Pedone, C., Scozzafava, A., Monti, S. M. & De Simone, G. (2009). *Proc. Natl Acad. Sci. USA*, **106**, 16233–16238.

Avvaru, B. S., Kim, C. U., Sippel, K. H., Gruner, S. M., Agbandje-McKenna, M., Silverman, D. N. & McKenna, R. (2010). *Biochemistry*, **49**, 249–251.

Barathova, M., Takacova, M., Holotnakova, T., Gibadulinova, A., Ohradanova, A., Zatovicova, M., Hulikova, A., Kopacek, J., Parkkila, S., Supuran, C. T., Pastorekova, S. & Pastorek, J. (2008). *Br. J. Cancer*, **98**, 129–136.

Benej, M., Pastorekova, S. & Pastorek, J. (2014). *Carbonic Anhydrase: Mechanism, Regulation, Links to Disease, and Industrial Applications*, edited by S. C. Frost & R. McKenna, pp. 199–219. Dordercht: Springer.

Carroux, C. J., Rankin, G. M., Moeker, J., Bornaghi, L. F., Katneni, K., Morizzi, J., Charman, S. A., Vullo, D., Supuran, C. T. & Poulsen, S.-A. (2013). *J. Med. Chem.* **56**, 9623–9634.

Domsic, J. F., Avvaru, B. S., Kim, C. U., Gruner, S. M., Agbandje-McKenna, M., Silverman, D. N. & McKenna, R. (2008). *J. Biol. Chem.* **283**, 30766–30771.

Emsley, P. & Cowtan, K. (2004). *Acta Cryst.* D**60**, 2126–2132.

Frost, S. C. (2014). *Subcell. Biochem.* **75**, 9–30.

Genis, C., Sippel, K. H., Case, N., Cao, W., Avvaru, B. S., Tartaglia, L. J., Govindasamy, L., Tu, C., Agbandje-McKenna, M., Silverman, D. N., Rosser, C. J. & McKenna, R. (2009). *Biochemistry*, **48**, 1322–1331.

Gill, S. C. & von Hippel, P. H. (1989). *Anal. Biochem.* **182**, 319–326.

Hilvo, M. *et al.* (2008). *J. Biol. Chem.* **283**, 27799–27809.

Laskowski, R. A., MacArthur, M. W., Moss, D. S. & Thornton, J. M. (1993). *J. Appl. Cryst.* **26**, 283–291.

Liao, S.-Y., Lerman, M. I. & Stanbridge, E. J. (2009). *BMC Dev. Biol.* **9**, 22.

Lopez, M., Paul, B., Hofmann, A., Morizzi, J., Wu, Q. K., Charman, S. A., Innocenti, A., Vullo, D., Supuran, C. T. & Poulsen, S.-A. (2009). *J. Med. Chem.* **52**, 6421–6432.

Lopez, M., Trajkovic, J., Bornaghi, L. F., Innocenti, A., Vullo, D., Supuran, C. T. & Poulsen, S.-A. (2011). *J. Med. Chem.* **54**, 1481–1489.

Luo, D., Wang, Z., Wu, J., Jiang, C. & Wu, J. (2014). *Biomed Res. Int.* **2014**, 409272.

Mahon, B. P. & McKenna, R. (2013). *Curr. Top. Biochem. Res.* **15**(2), 1–21.

Mahon, B. P., Pinard, M. A. & McKenna, R. (2015). *Molecules*, **20**, 2323–2348.

McDonald, P. C., Winum, J.-Y., Supuran, C. T. & Dedhar, S. (2012). *Oncotarget*, **3**, 84–97.

Métayer, B., Mingot, A., Vullo, D., Supuran, C. T. & Thibaudeau, S. (2013). *Chem. Commun.* **49**, 6015–6017.

Meyer, H., Vitavska, O. & Wieczorek, H. (2011). *J. Cell Sci.* **124**, 1984–1991.

Mikulski, R., West, D., Sippel, K. H., Avvaru, B. S., Aggarwal, M., Tu, C., McKenna, R. & Silverman, D. N. (2013). *Biochemistry*, **52**, 125–131.

Moeker, J., Mahon, B. P., Bornaghi, L. F., Vullo, D., Supuran, C. T., McKenna, R. & Poulsen, S.-A. (2014). *J. Med. Chem.* **57**, 8635–8645.

Moulder, J. E. & Rockwell, S. (1987). *Cancer Metastasis Rev.* **5**, 313–341.

Otwinowski, Z. & Minor, W. (1997). *Methods Enzymol.* **276**, 307–326.

Pastoreková, S., Parkkila, S., Parkkila, A. K., Opavský, R., Zelník, V., Saarnio, J. & Pastorek, J. (1997). *Gastroenterology*, **112**, 398–408.

Patterson, R. M., Selkirk, J. K. & Merrick, B. A. (1995). *Environ. Health Perspect.* **103**, 756–759.

Peskin, B. & Carter, M. J. (2008). *Med. Hypotheses*, **70**, 298–304.

Pinard, M. A., Boone, C. D., Rife, B. D., Supuran, C. T. & McKenna, R. (2013). *Bioorg. Med. Chem.* **21**, 7210–7215.

Pinard, M. A., Mahon, B. & McKenna, R. (2015). *Biomed Res. Int.* **2015**, 453543.

Racker, E. (1981). *Science*, **213**, 1313.

Schüttelkopf, A. W. & van Aalten, D. M. F. (2004). *Acta Cryst.* D**60**, 1355–1363.

Siebels, M., Rohrmann, K., Oberneder, R., Stahler, M., Haseke, N., Beck, J., Hofmann, R., Kindler, M., Kloepfer, P. & Stief, C. (2011). *World J. Urol.* **29**, 121–126.

Silverman, D. N., Tu, C. K. & Wynns, G. C. (1980). *Biophysics and Physiology of Carbon Dioxide*, edited by C. Bauer, G. Gros & H. Bartels, pp. 254–261. Berlin, Heidelberg: Springer.

Supuran, C. T. (2012). *J. Enzyme Inhib. Med. Chem.* **27**, 759–772.

Tafreshi, N. K., Bui, M. M., Bishop, K., Lloyd, M. C., Enkemann, S. A., Lopez, A. S., Abrahams, D., Carter, B. W., Vagner, J., Grobmyer, S. R., Gillies, R. J. & Morse, D. L. (2012). *Clin. Cancer Res.* **18**, 207–219.

Vander Heiden, M. G., Cantley, L. C. & Thompson, C. B. (2009). *Science*, **324**, 1029–1033.

Winum, J.-Y., Colinas, P. A. & Supuran, C. T. (2013). *Bioorg. Med. Chem.* **21**, 1419–1426.

Wykoff, C. C., Beasley, N. J., Watson, P. H., Turner, K. J., Pastorek, J., Sibtain, A., Wilson, G. D., Turley, H., Talks, K. L., Maxwell, P. H., Pugh, C. W., Ratcliffe, P. J. & Harris, A. L. (2000). *Cancer Res.* **60**, 7075–7083.